Water Resources Research

RESEARCH ARTICLE
10.1029/2019WR026673

Key Points:
- Gravity signals and water level data of 20 underground flash flood events are used to estimate their impact on the karst aquifer recharge
- The analysis of gravity data prior and after underground flood events does not suggest any significant recharge in the saturated zone the aquifer
- Forward gravity modeling of flood events affecting mapped caves evidences unknown cavities in the system

Supporting Information:
- Supporting Information S1
- Data Set S1
- Data Set S2
- Data Set S3

Correspondence to:
A. Watlet,
arnw@bgs.ac.uk

Citation:
Watlet, A., Van Camp, M., Francis, O., Poulain, A., Rochez, G., Hallet, V., et al. (2020). Gravity monitoring of underground flash flood events to study their impact on groundwater recharge and the distribution of karst voids. *Water Resources Research*, *56*, e2019WR026673. https://doi.org/10.1029/2019WR026673

Received 13 NOV 2019
Accepted 7 MAR 2020
Accepted article online 12 MAR 2020

Gravity Monitoring of Underground Flash Flood Events to Study Their Impact on Groundwater Recharge and the Distribution of Karst Voids

A. Watlet[1,2,3], M. Van Camp[2], O. Francis[4], A. Poulain[5], G. Rochez[5], V. Hallet[5], Y. Quinif[3], and O. Kaufmann[3]

[1]Multihazard and Resilience, British Geological Survey, Nottingham, UK, [2]Seismology-Gravimetry, Royal Observatory of Belgium, Uccle, Belgium, [3]Geology and Applied Geology Unit, Faculty of Engineering, University of Mons, Belgium, [4]Faculty of Science, Technology and Medicine, University of Luxembourg, Luxembourg City, Luxembourg, [5]Department of Geology, University of Namur, Namur, Belgium

Abstract Flash flood events are expected to become increasingly common with the global increases in weather extremes. They are a significant natural hazard that affects karst landscapes, which host large resources of drinking water worldwide. The role played by underground flood events in the karst aquifer recharge is complex due to the heterogeneity of the basement which remains poorly understood. We present the analysis of 20 incave flash flood events affecting the Rochefort karst system (Belgium) using continuous gravity measurements at one single station and water level sensors installed in caves. Underground flood events typically produce a peak in the gravity signal, due to an increase in the associated mass change. After the flood, the gravity values drop but remain slightly increased compared to before the flood event. Via forward gravity modeling, we demonstrate that this remaining anomaly can be reasonably explained by the infiltration of local rainfall within the karst system rather than by allogenic recharge of the aquifer. Flash floods are mainly restricted to connected voids. This allows us to utilize them as proxies to investigate the distribution of cavities in the karst system. Forward modeling of the gravitational attraction induced by the mapped caves being flooded yields a gravity signal much smaller than the observed one. We conclude that at least 50% more cavities than those previously mapped are required to match the measured anomalies. This presents opportunities for implementing similar approaches in other diverse porous media, using gravity monitoring of hydrological processes (e.g., infiltration fronts, hydrothermalism, or tide effects in coastal aquifers) as proxies to characterize underground properties.

1. Introduction

The distribution of flash flood events is expected to increase worldwide due to climate change (Hirabayashi et al., 2013). In karst landscapes, they are already considered one of the main hazards (Bonacci et al., 2006). Within few hours following intense rainfall events, storms, or rapid snow melting, underground conduits can be flooded, resulting in a peak discharge at the karst system outlet. These subsurface processes are often exacerbated by severe surface flood events. Due to their rapidity, the impact of underground flood events on the aquifer recharge is difficult to ascertain. Jourde et al. (2014) could identify three types of flash floods in a Mediterranean climate, classified as (i) floods mainly resulting in surface runoff across the hydrologic watershed, (ii) floods for which the karst aquifer can absorb some of the water excess, and (iii) floods which are combined with a groundwater contribution from the karst aquifer. The karst aquifer level is the identified main driver in each case. Depleted karst aquifers, as a result of a dry summer and/or due to high water abstraction rates, can potentially mitigate the effect of flooding at the surface. Such conditions are expected to vary from one type of karst to another and are likely to depend on climatic conditions.

Several specificities make karst hydrology particularly difficult to characterize and complex to model (Hartmann et al., 2014). Three types of permeability or porosity drive water circulation in karst aquifers: (i) micropores in unfractured carbonate rock matrix, (ii) tectonic joints or small fractures, and (iii) large karst conduits (White, 2002). Consequently, water circulation is highly heterogeneous in terms of flow types (Bakalowicz, 2005). Autogenic recharge mainly comes from rainwater infiltrating through the vadose zone, which results in a duality of flow types: slow seepage through the rock matrix and quick flows through

fractures and conduits (Atkinson, 1977; Smart & Friederich, 1987). In parallel, allogenic recharge results from rivers infiltrating karst landscapes through swallow holes and subsequent conduit networks (Goldscheider & Drew, 2007).

Understanding temporal and spatial variability of hydrological quantities is a key concept in hydrology (Blöschl & Sivapalan, 1995; Woods, 2006). The main problems in characterizing or modeling hydrological processes come from possible inconsistencies in extrapolating data from point-based observations in heterogeneous environments and/or inadequate temporal resolutions of measurements. Contemporary gravimetric techniques, due to their high resolution and integrative nature, are able to monitor hydrogeological effects at different scales (Van Camp et al., 2017). Terrestrial gravity measurements are appropriate for investigating local hydrological effects, whereas gravity data observations acquired by satellite (GRACE or GRACE-FO missions) are mainly applicable at large scales, that is, continental basins (Van Camp et al., 2014). Several studies demonstrated the use of time-lapse terrestrial gravity observations for monitoring groundwater content changes (Creutzfeldt et al., 2014; Imanishi et al., 2006; Takemoto et al., 2002; Wilson et al., 2012). Similar approaches were also developed to characterize hydrothermal processes (Caratori Tontini et al., 2016; Hemmings et al., 2016). Because of the integrated observations that they provide, gravity monitoring is particularly suitable to investigate karst groundwater systems, as already pointed out by Chalikakis et al. (2011). Some studies have successfully used time-lapse microgravity measurement to identify temporary groundwater storage in the karst vadose zone (Deville et al., 2012; Fores, 2016; Jacob et al., 2008). The high resolution of modern gravimeters, for example, superconducting gravimeters (SGs), typically reaches 0.1 nm/s^2 (0.01 μGal) (Van Camp, Meurers, et al., 2016), allowing subcentimetric variations in water height to be measured in the vicinity of the measurement site, as demonstrated by Van Camp, de Viron, et al. (2016). In practice, very small inaccuracies in applying atmospheric pressure corrections to gravity timeseries (Merriam, 1992) often reduce the resolution down to precisions of ~1 nm/s^2. Modeling hydrological effects when aiming at reducing them from gravity time series are complex (Creutzfeldt et al., 2010; Meurers et al., 2007; Mikolaj et al., 2015, 2019; Reich et al., 2019). Hence, highly local factors such as vegetation, hydraulic conductivity, bulk rock porosity, or the presence of underground cavities can have a large influence water storage and, consequently, local gravity variations. Assessing these factors is necessary in order to isolate the hydrological signature from other sources of gravity perturbations. Could gravity signatures of hydrological processes be used to inform on local subsurface properties? This question was addressed by Kennedy et al. (2016), in a study that estimated the hydraulic conductivity of the vadose zone using time-lapse gravity measurements of infiltration processes at an artificial recharge facility.

In this study, we present the analysis of 20 karst flash flood events in a humid karst landscape (following the classification of Hartmann et al. [2015]) using data from a combined gravity and hydrogeological monitoring campaign. We specifically investigate the effect of the floods on aquifer recharge. We also consider the recommendations of Kennedy et al. (2016), by demonstrating that continuous gravity measurements during natural hydrological processes could be used to investigate the distribution of voids in the near surface of the system.

2. Site Description and Hydrogeological Context

The site is located in the city of Rochefort (Figure 1b) (southern Belgium), part of the Variscan fold-and-thrust belt. The local geology consists of an overturned syncline, with high-dipping strata striking N070°E, comprising of outcropping Devonian limestones within shales to the south and shaly limestones to the north. Multiple karst systems exist in the area where the Lomme River, that originates in a plateau approximately 15-km south of Rochefort, crosses the limestone strata.

The outcropping geological layers and the karst system itself (Figure 1b) strongly influence the geomorphology of the studied area. To the South, a limestone plateau reaches 230-m above ordnance datum (AOD). A valley which follows the Lomme River bed and an ancient river channel incises the northside and the westside of the plateau, respectively. To the north, the Lomme valley opens on to a lowland area outcropping shaly limestone formations. Dye tracer tests have highlighted that the limestone layers are locally separated in to two distinct units by the Flohimont shales that act as an impervious layer (Poulain, 2017). Each unit contains a distinct cave system: the Lorette Cave in the south and the Nou Maulin Cave in the north. The

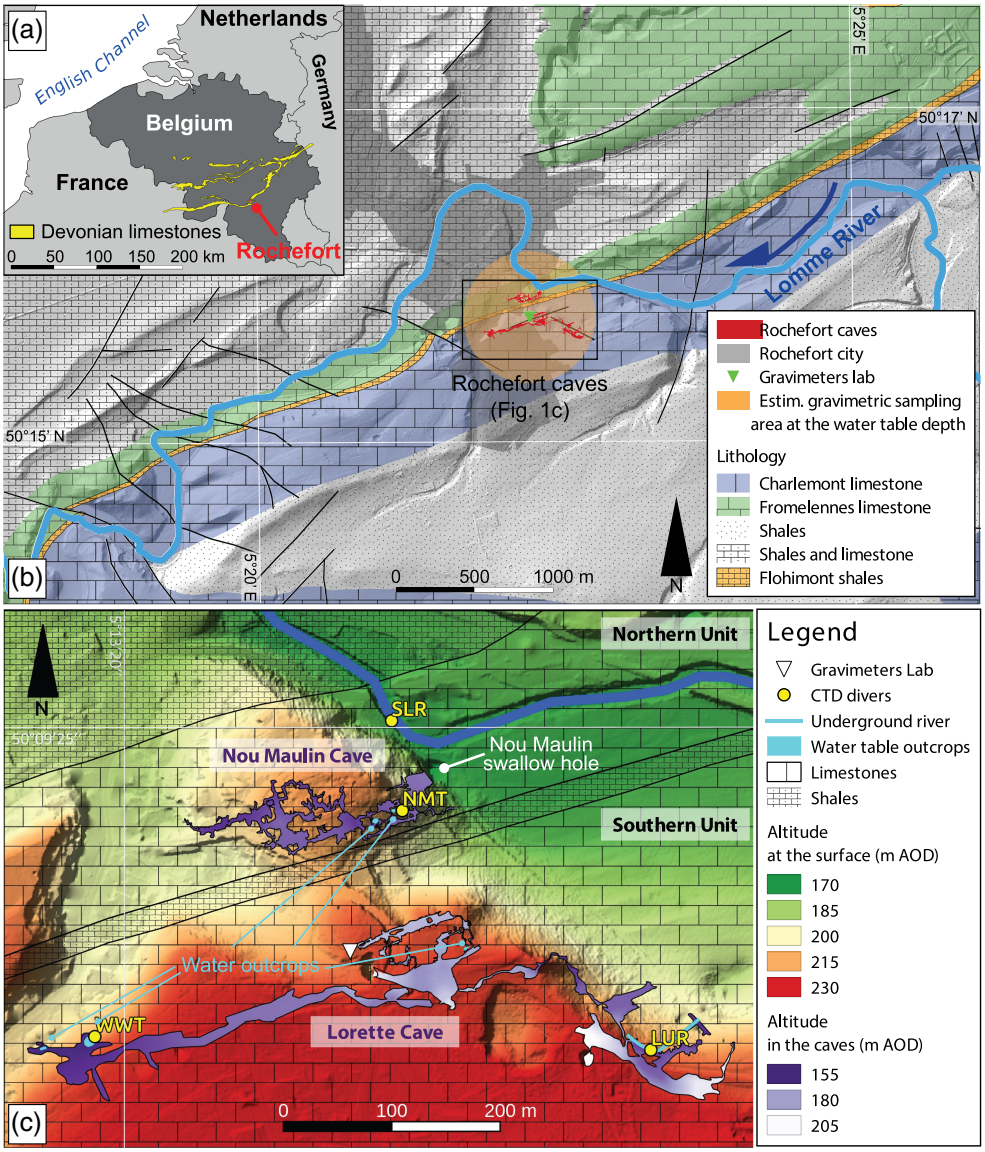

Figure 1. (a) General map of Belgium, showing the Rochefort region and the Devonian limestone crossing Belgium. (b) Geological overview of Rochefort region. The limestone units of the Calestienne are highlighted in green (Frommelennes limestone) and blue (Charlemont limestone). The impermeable Flohimont shales are also highlighted in yellow. The Rochefort caves are displayed, as well as the estimated gravimetric sampling surface of the gravimeter installed at RCL site, representing 85% of the Bouguer plate effect, at the depth of the saturated zone. The Gerny limestone massif is located on the northeast corner of the map. (c) Digital elevation model based on Lidar data of DGO3-SPW. Level of the bottom of the Lorette (Legros et al., 1993; Quinif, 2016) and Nou Maulin (Birkhoff et al., 2013; Dikstra & Burgers, 2015; Dubois, 1993) caves is illustrated. Outcrops of the shales layers within the limestone layers are overprinted in black (Barchy et al., 2014). Water-level sensors are labeled as west water table (WWT), Nou Maulin water table (NMT), and Lomme Underground River (LUR) for the incave monitoring and surface Lomme River (SLR) for the river monitoring.

Flohimont shales have an impact on the local geomorphology and form a gentle incision in the Limestone massif.

Near Rochefort, the limestone plateau is marked with three main sinkholes, two of which gives access to the Lorette Cave. The cave comprises a well-developed karstic network of large galleries. These large galleries have diameters of several meters and are oriented along the direction of geological strike, and smaller passages are orientated parallel to direction of geological dip. The eastern part of the cave contains a huge room (>20,000 m^3) and some lower passages. An underground river can be reached at around 162-m AOD (close to Lorette Underground River (LUR) station). The middle part of Lorette Cave is characterized by a large chamber called the Val d'Enfer (>10,000 m^3). It was formed as a result of a massive collapse which has

left two scree slopes on the sides of the cavity. This chamber opens on to small galleries in the north. Most of the central area is situated between ~180- and ~190-m AOD (40 to 30 m below ground level), while one single small gallery descends toward the water table outcropping at 162-m AOD. One single large passage composes the western part of the cave system, which follows the regional strike orientation. As indicated in Figure 1c, the gallery slopes downward to 170-m AOD where it opens to the western chamber, which itself steeply descends to 156-m AOD at which level the water table outcrops in two distinct locations. The whole cave is located in the Charlemont limestones (Figure 1b) which form the southern hydrogeological unit.

The floors of the Nou Maulin Cave are mostly lower than in the Lorette Cave, with an average altitude of ~165- to ~170-m AOD. It is located in the Fromelennes limestones, which form the northern hydrogeological unit. The cave constitutes the main swallow hole of the Lomme River although an artificially constructed dyke blocks the entrance most of the time (Van Camp et al., 2006). The entire riverbed is paved around Rochefort to ensure sufficient water supply during dry summers and is therefore perched and does not reflect the true water table level in this area.

Due to Belgium's temperate maritime climate, precipitations are evenly distributed throughout the year, and floods can occur at any time. Allogenic waters originating from the Lomme River flood both caves when the discharge exceeds 25 m^3/s (Figure 2). However, the floods are slightly delayed in the Lorette Cave because the main swallow hole of the Southern Unit is located 450-m upstream while that of the Nou Maulin Cave connects directly to its main galleries. This lag, which varies from 4 to 8 hr depending on the discharge of the Lomme River, is not the focus of this paper and is not considered in the analysis.

3. Methodology

3.1. Gravity Data Acquisition

This research benefits from the monitoring infrastructure of the Rochefort Cave Laboratory (RCL) site (Camelbeeck et al., 2011; Quinif et al., 1997). A small building houses the gravimeters in the top of the limestone massif next to a steep sinkhole that gives access to the central part of the Lorette Cave. In the surroundings of the building, there is a thin clayey soil layer of 20- to 50-cm thick overlaying the weathered limestone bedrock constituting the epikarst.

The building houses two vertical 1.5 × 1.5 m shafts, 2 m away from each other, which are dug into the bedrock (see www.karag.be for pictures). A concrete pier G1, leveled at the ground surface, hosts the absolute gravimeter (AG). A second pier (G2) (see Figure S1 in the supporting information) was leveled with concrete, in order to host the gPhone #032 relative spring gravimeter (GG) from Micro-g LaCoste and later the iGrav #019 SG from GWR, 1-m below ground level.

The GG was operational from 23 October 2013 to 20 November 2014 in the surface lab of RCL at location G2. It was replaced by the SG which became operational on 16 December 2014. This gravimeter has continuously measured ever since. The AG is portable and measures approximately 15 times per year, at location G1. The AG data are required to calibrate the relative gravimeters and verify and correct their instrumental drifts.

3.2. Gravity Data Processing, Noise, and Error Assessment

Processing the gravimeter time series includes correcting for tidal, atmospheric, and polar motion effects. The instrumental drift of the GG and the SG are corrected using the AG data; the GG experiences drifts of approximately 1.5×10^4 $nm.s^{-2}$/month, and the SG experiences drifts of a few dozens of $nm.s^{-2}$/year. These values are comparable to other gravitational studies (Sekowski et al., 2016). A detailed explanation of the drift correction applied to the SG (including the correction for some other instrumental steps) is provided in the supporting information (Text S1; Hinderer et al., 2007). Corrections applied to the SG are detailed in Francis et al. (2004) and to the AG in Van Camp (2005). The process of combining SG and AG data is detailed in Van Camp et al. (2013), with improvements demonstrated in Van Camp, Meurers, et al. (2016).

Global atmospheric pressure effects are corrected using mGlobe software (Mikolaj et al., 2016), which is based on global meteorological data from the ERA-interim model from ECMWF. Because these large scale models are limited to periods of 6 hr, following the advice detailed in Mikolaj et al. (2016), we apply an additional admittance factor to the difference between measured in situ atmospheric pressure and modeled local

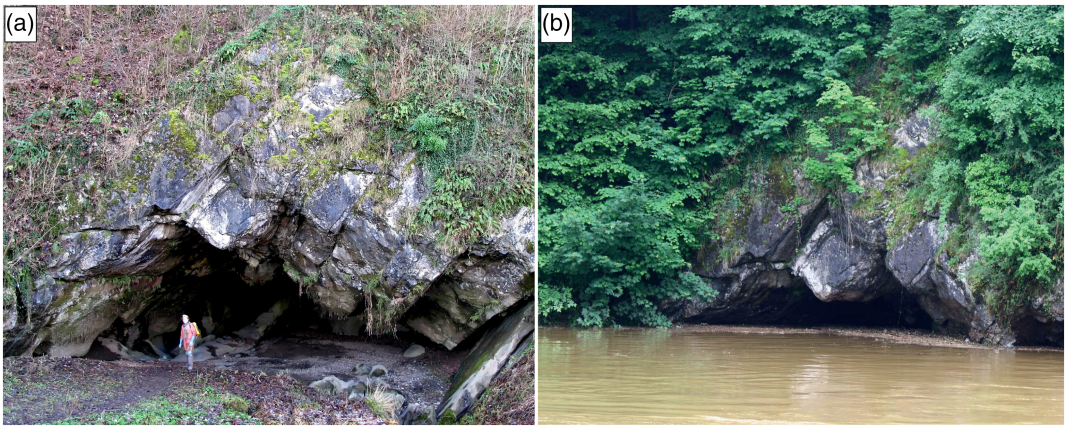

Figure 2. The Nou Maulin swallow hole (see location in Figure 1c) in dry (a) and flood (b) conditions. Photos credits: G. Rochez, A. Watlet.

pressure. This linear admittance factor is calculated during the tidal analysis process (Merriam, 1992). At Rochefort, the admittance factor calculated over the 3.8 years of gravity monitoring is −2.95 nm.s^{-2}/hPa. Due to the existence of a sinkhole and large cavities near the gravimeter, we modeled the effect of the local topography on the atmospheric pressure admittance. The vertical potential of the gravitational attraction is calculated for different local atmospheric pressures. No significant effect on gravity from the presence of air at altitudes below the gravimeter is deduced from these calculations (~0.002 nm.s^{-2}/hPa). A minor part of the local gravity variation is also related to continental hydrological effects. Gravity residuals are corrected for such effects using the same mGlobe software. The nonlocal hydrological effects calculated for the RCL site have a peak amplitude of ~4.5 nm.s^{-2}/year, which corresponds to ~10% of that of the measured gravity residuals (as seen in Figure 3a).

Power spectral densities (PSDs) of the gravity residuals during quiet days provide the noise level of the gravimeters. PSD are equal to 400 and 6 (nm.s^{-2})^2/Hz, for the GG and the SG, respectively. At 120-s period, which is the smallest time increment considered in this study, this corresponds to standard deviations of 1.4 and 0.2 nm.s^{-2}. The PSD of the SG (iGrav #019) compares well with that of the iGrav #002, which is also installed in karst environments (Fores et al., 2016) and corresponds to the expected instrumental precision (Warburton et al., 2010). The PSD of the GG (gPhone#032) is, however, 1 order of magnitude lower than the level reported by Riccardi et al. (2011) for the gPhone#054. This is because the GG installed at RCL site is provided with an active tilt control system, which eliminates spurious signals caused by slow tilting of the instrument (Fores et al., 2019). Without the tilt compensation, the observations of the GG could not be used in this study.

In this study, because flash floods are impulsive events lasting 2 to 4 days, it is important to characterize the environmental noise produced by external factors that affect the gravity during these events. Such noise can either come from imperfectly corrected tidal and/or atmospheric pressure effects, combined with longer term local or regional hydrological processes. Our approach consists of computing the rolling standard deviation (σ) across a moving 3-day window. The median standard deviation of this series results in 2.1 and 1.6 nm.s^{-2} for the GG and SG, respectively. The 2σ threshold (4.2 and 3.2 nm.s^{-2} for the GG and SG, respectively) provides a reasonable empiric estimation based on observed noise for characterizing flash flood events at the RCL site, as investigated in Mikolaj et al. (2019).

3.3. Gravity Modeling

In this study, we present modeling results calculated using the prism approach (Heck & Seitz, 2007). This approach is theoretically more accurate, especially at small scales, than other approaches commonly used for calculating topographic reductions in field gravity modeling (Leirião et al., 2009). Other such approaches include the point mass approximation or the MacMillan approach (MacMillan, 1958). This is based on the calculation of the vertical component of gravitational attraction, expressed for a body V in Cartesian coordinates xyz, with a uniform density ρ. This is computed, at the origin, as follows:

$$g = G\iiint_V \rho\left(x^2 + y^2 + z^2\right)^{-1/2} dxdydz \quad (1)$$

Solving equation 1 can differ by the arcsine or arctangent approaches when deriving the gravitational attraction equation (e.g., Nagy, 1966; Okabe, 1979). Li and Chouteau (1998) provide a detailed review of the problem and found that the forward modeling of Okabe (1979) is one of the most reliable analytical solution of equation 1 (see details in supporting information Text S2), which we use here.

In order to accurately compute the gravity effect, we construct a mesh of hexahedra celles (3-D cubic prisms). The topography is derived from a regional Digital Elevation Model (DEM) provided by the Walloon regional institute DGO3-SPW. This airborne LIDAR data-based DEM is provided with a planar accuracy of 1 m and a claimed absolute elevation accuracy of 0.12 m throughout the covered territory (16,800 km^2). This resolution is sufficient for gravity modeling purposes when the focus of investigation is on hydrological processes, as discussed in detail in Creutzfeldt et al. (2008).

To adequately choose the extension of the mesh, one can refer to the Bouguer plate approximation. The Bouguer plate model estimates the anomaly δg in the vertical component of the gravity associated to a mass change, such as

$$\delta g = 2\,\pi\,\rho G H \quad (2)$$

where G is the gravitational constant, H is the thickness of an infinite plate, and ρ the density of the plate. This first approximation works well for large bodies but becomes ineffective when modeling local targets with limited extensions, for example, small groundwater reservoirs. From equation 2, it was demonstrated that the gravimetric sampling volume below a gravimeter can be represented as a cone with a basis diameter significantly larger than its height (Deville, 2013; Van Camp et al., 2017). The sensitivity of the gravimeter decreases logarithmically with depth, with deeper masses sampled across a plane with increasing diameter. Because the gravimeter is sensitive to the vertical component of the gravitational attraction, the further the lateral distance from the center of this cone, the lower the contribution to the gravity signal. At the RCL, the water table lies 58 m underneath the gravimeter; below this level, no water storage changes (WSCs) responsible for gravity variations may occur. At this level, a cone with a diameter of 800 m centered on the gravimeter delineates approximately 85% of the mass changes that can be detected with the SG. Figure 1b shows the base of this cone at the saturated zone level together with the geological information. Given the dimensions of this cone, all the known cavities of the Rochefort caves are well covered by the gravimetric monitoring. Figure 1b shows that the Gerny limestone massif northwest of Rochefort, which hosts a large aquifer, has no significant impact on the gravimetric data.

Based on these estimations, the bounding box for the prism modeling was set to 800 × 800 × 100 m. No significant hydrological variations are expected to occur outside this area, where mostly impervious shales outcrop. In the z direction, the box ranges from 250- to 150-m AOD, which correspond respectively to the highest point in the topography, and 2 m below the lowest water table level, below which no hydrological variations are expected. The DEM was discretized in a mesh comprising cells with a size of 0.25 × 0.25 × 0.25 m in the central part (a box of 60 × 60 m centered on the gravimeter) and 1 × 1 × 1 m^3 in the external part, which results in a final mesh with 2.7×10^7 cells.

The vertical component of gravitational attraction is calculated for each cell, for which a given WSC in terms of volume of water per cell is calculated using the density of water (1,000 kg/m^3). The modeled gravity change (Δg) at the position of the gravimeter is finally derived by summing the gravitational attraction of the whole set, or subsets of cells, following equation 1. Subsets of cells can be defined based on a-priori geological information. For example, cells attributed to shale layers have only a small impact on the gravity signal (<10% of the total gravity response) and are not taken into account in modeling karst water recharge, as they are considered to act as impervious layers in terms of groundwater storage. The Python source code developed for this modeling approach is available at https://gitlab.com/awatlet/pymodg website.

This study aims to incorporate the effects of cavities in the gravity modeling. The numerous mapping surveys of the caves (compiled in Birkhoff et al. [2013], Dikstra and Burgers [2015], Dubois [1993], Legros et al. [1993], and Quinif [2016]) provide topographical information on the lateral and vertical extents of

the passages (Figure 1c). Most of the speleological techniques lack accuracy, consisting of relatively simplistic approaches, for example, use of compass and (electronic) distometer and/or altimeter. We estimate a precision of 1 m (both in vertical and horizontal) in most of the areas and a conservative value of 5 m for the vertical information in the areas mapped longer ago, that is, the eastern part of Lorette Cave.

While sufficient information exists for the floors and walls of the known cavities, the position of the cavity roofs could not be precisely mapped with these techniques. However, in order to insert the cavities in the mesh, estimating their size is necessary. For the *Val d'Enfer* room, we use a 3-D photoscan model (Triantafyllou et al., 2019) to estimate the elevation of the roof. For other passages, the elevation of the roof is estimated as a function of their width in planar coordinates, resulting in cavities with heights ranging from 1 to 3 m for the thin and elongated passages and from 5 to 25 m for the larger rooms.

It is important to consider that the building hosting the gravimeter acts as a barrier to infiltration of rainwater in the soil during rainfall events. It has been shown that this process may reduce, or delay, the expected Δg associated with a rainfall event, known as the umbrella effect or the building mask (Creutzfeldt et al., 2008; Deville et al., 2012). At the RCL site, the gravimeter is installed in a 1-m deep shaft, which limits its sensitivity to the superficial layer. This is due to the fact that masses in the first meter below the ground surface in the vicinity of the gravimeter are at higher level than the gravity sensor and thereby yields a negative vertical attraction which mitigates the positive vertical attraction of superficial masses located further downslope. Gravity modeling shows that setting a depth below the building in which no soil moisture variation can occur to 2-m depth, as Güntner et al. (2017) did, has a limited impact on the response of the gravimeter to WSC in the first meters of the subsurface. Taking a building mask of 2-m depth reduces the modeled Δg by less than 25% for WSC in the first 3 m and by 10% only in the first 6 m. Practically, the building mask is expected to diminish in the hours following a rain event as rainwater starts percolating through cracks and beddings below the building and into deeper layers. However, the extent of the building mask in time is unknown, and is not the subject of this study, This is why, for the later analyses in this paper, we deal with modeled gravity values that are the mean value between gravity modeled with and without a building mask, within a confidence interval set as the difference between the two.

3.4. Hydrological Monitoring

The hydrological monitoring is performed using three CTD-Diver® pressiometric probes (measuring water level, electrical conductivity, and temperature) from Schlumberger Water Services (Figure 1c) installed in caves (LUR; Nou Maulin water table, NMT; West Water Table, WWT). They provide data at a 15-min sampling rate. The water pressure and corresponding water level are measured with a 10-cm maximum precision and long-term stability, as well as a 1-cm resolution. The data are corrected for the effects of air pressure with a Baro-Diver characterized by 2-cm precision and a 0.1-cm resolution. The level of the Lomme River is monitored hourly by the Walloon regional institute (DG03-DRCE-DCENN) in the city of Rochefort. All data are available in the supporting information.

A Lufft tipping bucket type rain gauge installed adjacent to the gravimeter laboratory measures precipitation every minute.

4. Results

4.1. Gravity and Hydrogeological Data Sets

We use 3 years and 8 months of continuous gravity data acquired from the RCL monitoring network, commencing in November 2013 and lasting up to July 2017. This data set shows an obvious seasonality (Figure 3a). Seasonal gravity changes recorded by SGs have already been explained by long-wavelength water storage variations (Boy & Hinderer, 2006). The variability in phase and amplitude in long gravity time series reflects the predominance of a local component in the hydrological signature, as already observed at several observatory stations (Creutzfeldt et al., 2010; Hasan et al., 2008; Lampitelli & Francis, 2010; Longuevergne et al., 2009; Naujoks et al., 2010; Van Camp et al., 2006, 2014). In Rochefort, the seasonal variation in the gravity data set has been interpreted as being mainly related to the local hydrology (Watlet, 2017). The data set also exhibits >20 high frequency peaks that are related to the flash floods occurring in the caves.

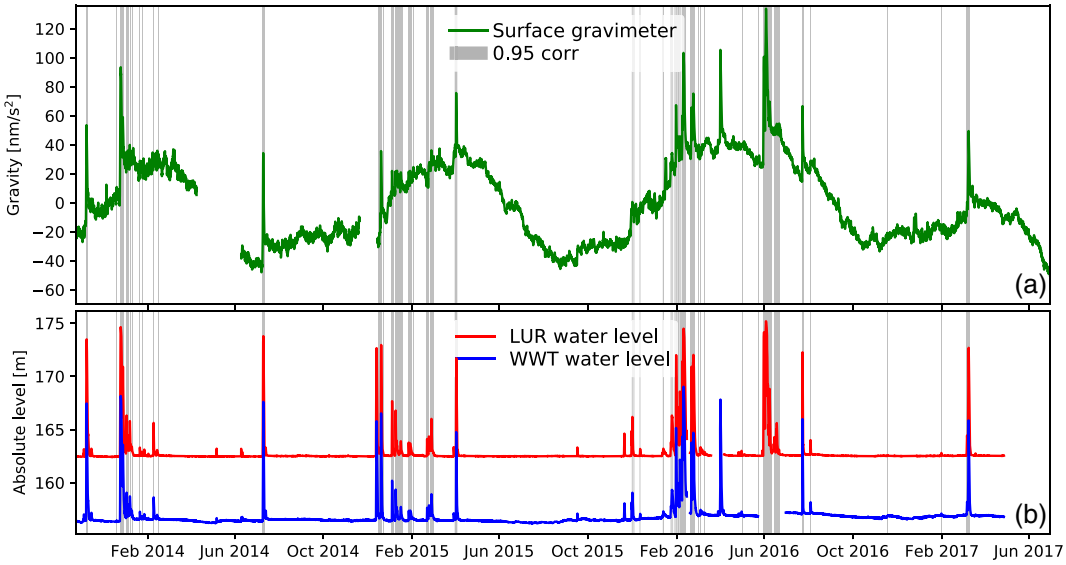

Figure 3. (a) Relative gravity measurements (green) observed at the RCL site. Tidal, atmospheric, polar motion effects, and instrumental drift are removed. For legibility, the average value of the gravity at Rochefort site is removed. A power outage occurred on 8 April 2014 and lead 2-month relaxation of the GG. The SG was installed on 16 December 2014. (b) Water levels of the west water table (WWR) and the Lomme Underground River (LUR) stations. Gray spans identify periods associated with rolling correlation (with a sliding window of 24 hr) greater than 0.95.

Figure 3b presents the hydrogeological data set overlapping the gravity monitoring period. Flash flood events with measured amplitudes larger than 3.5 m show the best correlation (Pearson's correlation coefficient $r > 0.95$) with the gravity timeseries. Some of the smaller flash flood events are also highly correlated ($r > 0.95$), although associated with small gravity variations (<5 nm.s^{-2}) that fall below the 2σ noise level ascertained for both the GG and SG data sets. Such events are therefore not taken into account in further analyses.

4.2. Flood Events Data

During flood events, high-frequency peaks in the water-level data are correlated with increased gravity measurements. Our data set comprises 20 flood events affecting the deepest parts of the Rochefort caves. They are detected both by the water level sensors and the gravimeter. They correspond to water level increases ranging from 3.5 to 13 m.

Figures 4c and 4d show data from the different water level probes (NMT, LUR, WWT, and SLR) and of the surface gravimeter during two floods in July 2014 and in April 2015, respectively. Figure 4c shows data from the GG while Figure 4d displays data from the SG, highlighting the lower instrumental noise of the latter. These two flood events differ from their amplitude. The flood event in July 2014 reached 11.3 m at LUR station (Figure 4c) while that of April 2015 only reached 9.1 m at LUR (Figure 4d). In both cases, the NMT signal (northern unit) is slightly out of phase compared to LUR and WWT signals (southern unit). However, this study will not focus on the transient signal associated to the flood events. Instead, the relationship between the gravity and the water levels will be investigated as if they were in steady state, which allows the structure of the limestone massif to be characterized.

The dynamics of the floods exhibit typical patterns in terms of measured water level and discharge; after a rapid increase of the level due to a flood event, the pressure head shows a nonlinear decrease and usually stabilizes, 20 to 50 cm above the level prior to flood. Then, usually after 48 hr, there is a slow linear decrease, lasting up to several days. Such a behavior is typical of karst environments and is described by Mangin (1975) as (i) a rapid flow of autogenic water from the vadose zone and allogenic water transiting in the epiphreatic zone exhibiting a non-linear recession and (ii) a delayed flow from slowly infiltrating water showing a linear baseflow recession. Such small shifts in the water levels prior and posterior to the flood events highlight the likely limited effect of the flood to recharge annex-to-drain systems of the epiphreatic zone.

The gravity increase follows the rising water levels. However, the gravity level reached after the flood, that is, after the rapid decrease, remains relatively high when compared with the water level (>15% of the amplitude

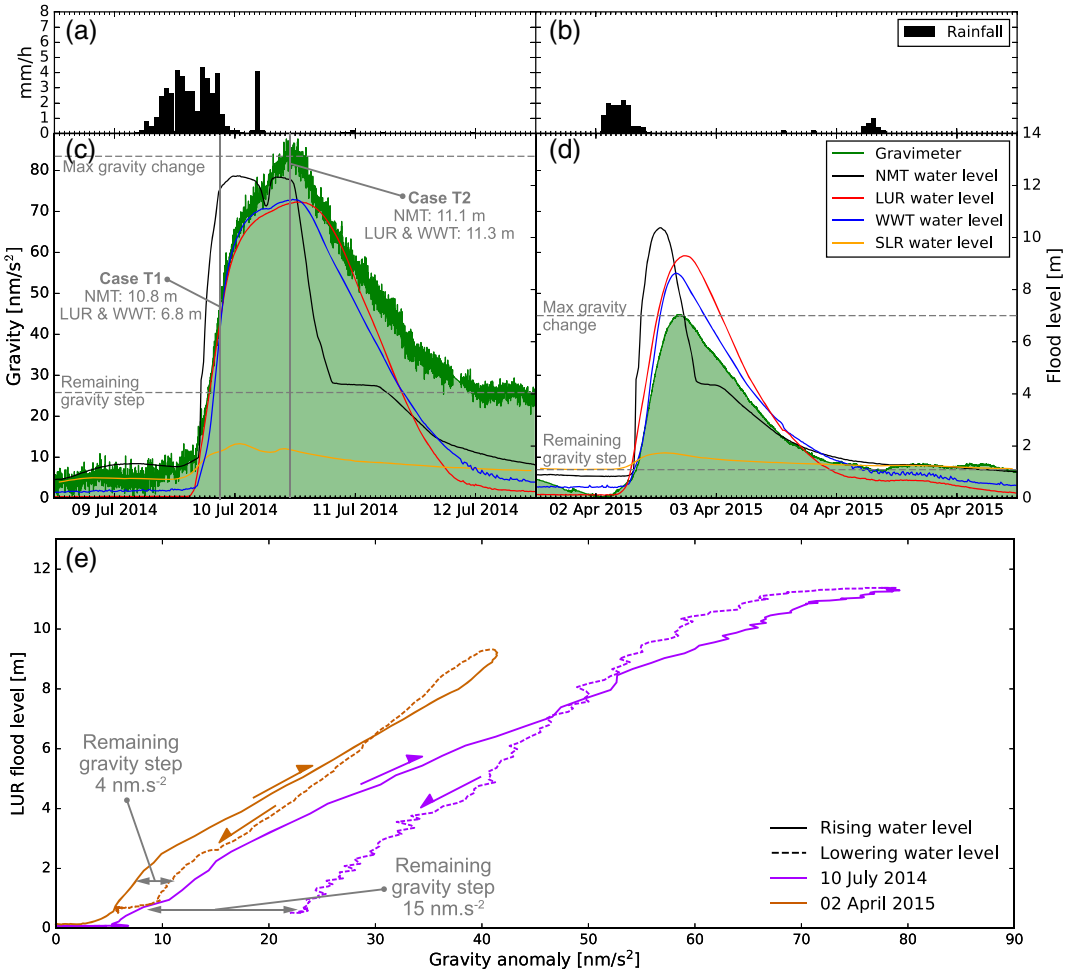

Figure 4. Precipitation (a and b), gravity, and relative water level data (c and d) during two flash flood events in December 2013 (a and c; GG) and April 2015 (b and d; SG). The greater gravity signal to noise ratio in (a) is due to the lower noise of the SG compared to that of the GG. (e) Plot of the LUR water level data against the relative variation of gravity for the two same flood events. The shifts in gravity values between the rising and the lowering water level of both flood (4 and 15 nm.s^{-2}) are highlighted.

of the gravity peak). This gravity step may have several explanations and is discussed in detail in the following section. During the flood itself, the gravity signal is closely matched to the water levels measured in the Southern Unit (Lorette Cave, LUR and WWT sensors). This is less obvious for the northern unit (Nou Maulin Cave, NMT sensor). For the July 2014 flood, when the level of the NMT probe approaches 11 m (Case T1 in Figure 4c), levels of LUR and WWT are only at 6.8 m and the gravity anomaly is identified at 42.5 ± 2.1 nm.s^{-2}. As the level stabilizes in the northern unit, the gravity anomaly continues increasing up to 71.0 ± 2.1 nm.s^{-2} following the rising water level in the southern unit from +6.8 to +11.3 m (Case T2 in Figure 4c). The rising water level in the northern unit (Nou Maulin cave) does not produce a similar increase in the gravity data to that seen in the Southern Unit (Lorette cave). This is not surprising, as the widths of the outcropping limestones in northern and southern units are 150 and 565 m, respectively, within vicinity of the gravimeter. This impacts the proportion of each unit in the sampling volume of the gravimeter (Figure 1a) at the depth of the saturated zone: 23.3% for the northern unit and 76.7% for the southern unit. Similar observations can be made in April 2015 and for all the other flash flood events not shown in Figure 4.

Figure 4e presents the gravity variation against the water level reached during these two flood events at the LUR station. These cases are representative of the 20 other flood events (see summary in Table S1 in the supporting information) and reveal two main pieces of information: (i) that at similar water levels during

Table 1
Modeled Δg Induced by a WSC of 1 mm Distributed in a Progressively Thicker Layer Below Topographic Surface Following the Approach Presented in Section 3.3

Thickness from the surface (m)	Δg (nm.s^{-2}/mm)
1	0.04 ± 0.03
2	0.20 ± 0.06
3	0.30 ± 0.04
4	0.34 ± 0.03
5	0.37 ± 0.02
6	0.39 ± 0.02

the increase, flood of July 2014 shows a greater gravity anomaly than that of the April 2015 flood, and (ii) that the gravity record does not show similar values for equal water levels of the rising and the lowering stages. The slight decrease in gravity associated with a stationary water level at the maximum flood amplitude is attributed to the phase shift between the southern and the northern units. As the water is still at the maximum measured level in the Lorette cave, the water level has already significantly dropped in the Nou Maulin cave, influencing the gravity signal. The offset between the gravity anomalies measured during the increasing and decreasing water level shifts afterward to positive values. It reaches +4 nm.s^{-2} for the April 2015 flood and +15 nm.s^{-2} for the July 2014 flood as highlighted in Figure 4e.

5. Discussion

5.1. Analysis of the Flood Events

We have seen that the gravity signal is sensitive to the increase of water levels measured in the caves during flood events. However, assessing the contribution of the local rainfall infiltration in the measured gravity signal is crucial in order to derive the actual gravity increase related to the flood process itself. The remaining gravity steps, after every flood event, as shown in Figure 4, have two possible explanations: (i) They result from the gravity loading produced by meteoric water still infiltrating the vadose zone after a flood event has terminated, or (ii) they reflect allogenic recharge of the annex-to-drain system in the epiphreatic zone as a consequence of the flood itself. Investigating the validity of the first scenario, that is, assessing if rainwater infiltration can be responsible for the remaining gravity step, has a direct influence on the likelihood of the second scenario.

Gravity changes associated with rainfall events are well-known effects (e.g., Fores et al., 2016; Imanishi et al., 2006; Meurers et al., 2007). The ratio between the gravity change and the intensity of the rainfall invent is often called rainfall admittance. It is site dependent, being influenced by local topography, soil properties, and characteristics of the gravimeter installation. Ultimately, the soil hydraulic conductivity and evapotranspiration are the crucial parameters that governs rainfall admittance factors, because it affects the depth reached by rainwater a certain amount of time after a rain event. In karst areas, how fast and how deep rainwater infiltrates the superficial layers is a key question. Given the duality of flow types affecting karst systems (Atkinson, 1977; Smart & Friederich, 1987), a part of the infiltrating water rapidly percolates through open cracks toward deep layers, while the remainder is delayed as it percolates through the shallow epikarst. This has been highlighted at the RCL site by Poulain et al. (2018) via an incave percolating water monitoring experiment. They emphasized that rainfall is followed by quick flow discharge in the roofs of the RCL cave located 20 m below the surface. They also demonstrate that this quick flow component generally last for 2 days, after which a diffuse flow component attributed to the seeping of water delayed in the epikarst, predominates and lasts for more than 10 days. This delayed infiltration in the epikarst has also been confirmed at the RCL using a long-term Electrical Resistivity Tomography monitoring (Watlet et al., 2018).

At Rochefort, allogenic floods are generally associated with intense local rainfall events, due to the location of the RCL close to the source of the Lomme River, and in turn to all the upstream catchment areas. Such rainfall events start several hours before the river swells and ultimately infiltrates the cavities. The floods themselves last 1 to 3 days, as long as the level of the surface river is high enough to feed the swallow holes, and depending on the length of the rain event. Conducting a classical study on the effects of local rainfall to the RCL gravity signal recorded at the surface is rather complex for two main reasons.

First, sensitivity of the gravimeter to the uppermost layer is very low, due to the installation of the gravimeter below the ground surface. Table 1 displays the modeled gravity effect of a 1-mm rain event stored in superficial layers of variable thickness, following the approach presented in section 3.3. It shows a very low admittance of 0.04 ± 0.03 nm.s^{-2} per millimeter of water spread in the first meter of the subsurface. This value quickly increases when considering that rainwater infiltrates toward greater depth. This suggests that low-magnitude rainfall events are barely detectable in the gravity signal, which is confirmed by the actual gravity data.

Second, higher magnitude rainfall events often trigger underground flood events at the RCL site, which have both an effect on the gravity signal and makes it difficult to assess a direct gravity changes associated with rainfall events.

Is the gravity step posterior to each flood event induced by allogenic recharge of the aquifer or by an increase in the water content of the vadose zone, due to delayed rainwater infiltration? Figure 5 shows the relationship between the rainfall intensity and the remaining gravity step. Because the delay of the gravity response to rainwater infiltration is not known, rainfall intensity is calculated as the mean between rainfall intensity starting 1 day up to the end of each flood and that starting 3 days up to the end. Horizontal error bars in Figure 5 represent the difference of rainfall intensity following one or the other approach. We fitted an orthogonal distance regression (Boggs et al., 1992), which takes into account errors in both coordinates. The slope of the fitted model, hence, the fitted rainfall admittance factor, equates 0.34 ± 0.6 nm.s^{-2} per millimeter of water. When looking at the period of the year of each flood, the summer floods are slightly below this threshold, whereas only winter heavy rainfall events are above this threshold. This suggests that rainwater infiltrates deeper in the massif in winter than it is the case in summer, which is expected given the summer vegetation acts to decrease water infiltration. Moreover, dry clayey soils may experience increased runoff, decreasing actual rainwater infiltration. In any case, more observations are required to confirm this interpretation.

Using the 3-D modeling presented in section 3.3, we can investigate the significance and, thereby, the validity of such a rainfall admittance in terms of average infiltration depth within the shallow layers. Table 1 shows that the value of 0.34 ± 0.6 nm.s^{-2} per millimeter of water as rainfall admittance corresponds to an impacted depth between 3 and 5 m. This matches the depth of the epikarst at the RCL site. In reality, it is likely that rapid percolation through open cracks brings parts of the rainwater in deeper layers. This would counterbalance and, thus, raise the gravity response given that the gravimeter is more sensitive to deeper areas. In other words, the average superficial layer responsible for most of the temporary storage of the rainwater might be slightly thinner than the 3- to 5-m-modeled depth.

Note. Δg are shown as the mean between models with and without building masks, while the error reflects the interval between the two.

To validate this result, we focus on a second independent approach comparing the relationship between the amplitude of the flood and its associated gravity anomaly. This is taken as the difference between the maximum gravity value and either (i) the starting value (Δg_{start_max}) or (ii) the final value (Δg_{end_max}). The main assumption is that

$$\Delta \boldsymbol{g}_{\boldsymbol{end\_max}} = \Delta \boldsymbol{g}_{\boldsymbol{start\_max}} - \Delta \boldsymbol{g}_{\boldsymbol{rainfall}} = \Delta \boldsymbol{g}_{\boldsymbol{start\_max}} - \boldsymbol{k}.\boldsymbol{P} \tag{3}$$

where P is the precipitation associated to each flood expressed in mm of water and k the rainfall admittance. We use a fitting approach which consists in minimizing the rainfall admittance value k to reproduce the actual Δg_{end_max}. The rainfall is once again taken as the average precipitation measured 1 to 3 days prior to each flood. A thousand values of admittance ranging between 0 and 0.42 nm.s^{-2} per millimeter of water are tested. The value showing the lowest Root Mean Square Error (RMSE) is selected as best fit, in this case, 0.32 nm.s^{-2} per millimeter of water (see Figure S2). This is very similar to results obtained with the first approach (Figure 5), thereby confirming that rainwater infiltration explains the gravity increase remaining after the flood event.

By using two independent approaches, we can validate the assumption that rainwater loading is largely responsible for the gravity step posterior to the flood event. As a direct consequence, this also demonstrates that RCL gravity data does not support the hypothesis that underground floods may result in any significant recharge of capacitive subsystems in deep sections of the aquifer. Instead, the results suggest that the flood events are predominantly confined in macroscopic conduits and connected voids. In Rochefort, the 20 investigated flash floods are short-lived events, marked by piston-like water invasion that could not significantly recharge capacitive areas of the limestone massif. This differs from the study of Jourde et al. (2014) which identified some floods leading to aquifer recharge, in a Mediterranean context. In their case, the aquifer shows large seasonal variations. A depleted aquifer is prone to absorb flash flood water more readily. Conversely, in Rochefort, the level of the aquifer is stable throughout the year, and there is no evidence of different behavior in terms of recharge of the aquifer between summer and winter floods.

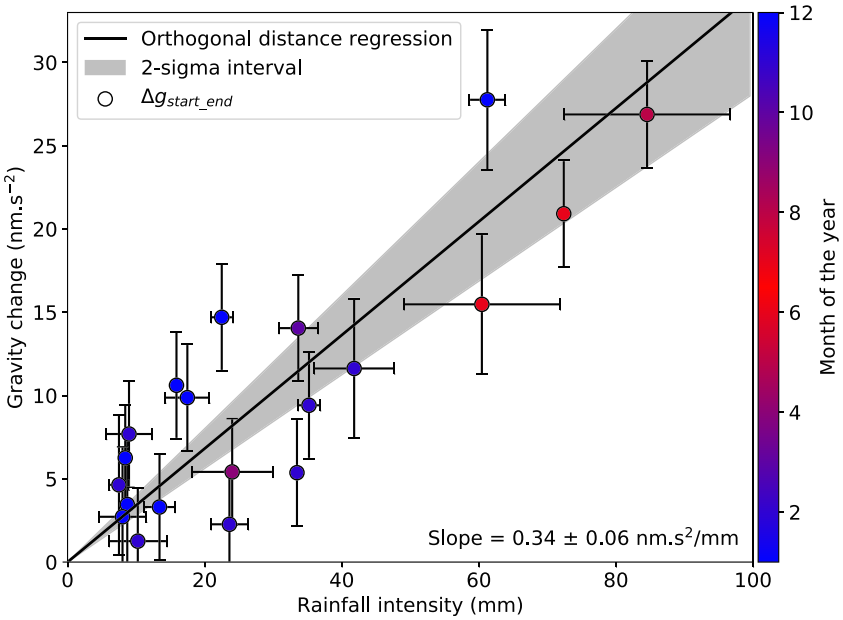

Figure 5. Gravity step reached after each flood as a function of concurrent rainfall intensity. The black line represents a linear regression constrained through the origin. Horizontal error bars highlight the error estimate on the gravity data set, as defined in section 2, and the vertical error bars represent the variation in rainfall intensity when summing over periods starting 1 or 3 days prior to the beginning of each flood, with the point located at the mean. Points are colored according to the period of the year during which the flood occurred, with red colors corresponding to summer and blue colors to winter.

5.2. Estimation of Karst Voids

The analysis of water level and gravity data shows that the floods are mainly limited to transmissive conduits. Therefore, the extension of the flood events in the limestone massif and the associated increase of water masses detected by the gravimeter are key elements to inform on the amount of connected voids that can be accounted for in the studied area. As is typical in karst systems, a certain number of the underground conduits remain unknown or inaccessible. We investigate hereafter whether gravimetric monitoring can reveal such unknown extensions.

Figure 6a summarizes the 20 flood events by plotting the gravity difference and the highest water level reached during each flood for the three underground stations. Data are showing a similar nonlinear relationship, already discernible from the data of the July 2014 flood in Figure 4e. Three points from NMT station seem slightly offset with remarkable gravity anomalies for very low measured water levels (<3 m). These can be explained by the fact that the Nou Maulin swallow hole is protected by an artificial 2-m dyke which prevents smaller floods from filling the cave. In such cases, NMT water level signal is only impacted by an input of water coming from minor swallow holes in the northern unit dispatched upstream of this main one. Conversely, the gravity signal is already impacted by floods largely affecting the Lorette cave, due to the presence of larger swallow holes upstream in the southern unit. Because of this particularity of NMT, we decide to focus mainly on water level data measured in the Lorette cave for the remainder of this study.

First, we simulate the gravity response of floods restricted to the mapped cavities of Lorette Cave and Nou Maulin Cave (Figure 6c). As mentioned in section 3.3, a thickness of 1 to 3 m was assigned to the smaller conduits, while 5 to 25 m was assigned to larger conduits, following the circular shape of the cavities. The simulations demonstrate that the model is not able to describe well the gravity anomalies associated with floods restricted to the mapped cavities. To fit the observations, adding voids to the karst system is required. As it is not possible to know the exact location of these unknown cavities, we have considered a first simple case where the voids are uniformly spread as an average porosity in the massif. When considering a repartition of voids in the area comprised in the highest sensitivity zone of the gravimeter (radius of 400 m around the gravimeter, as explained in section 3.3), we find a total amount of 78,520 m^3 of voids in addition to the modeled mapped passages which amounts 26,260 and 11,750 m^3, respectively, for Lorette Cave and Nou Maulin Cave in the slice where the floods occur.

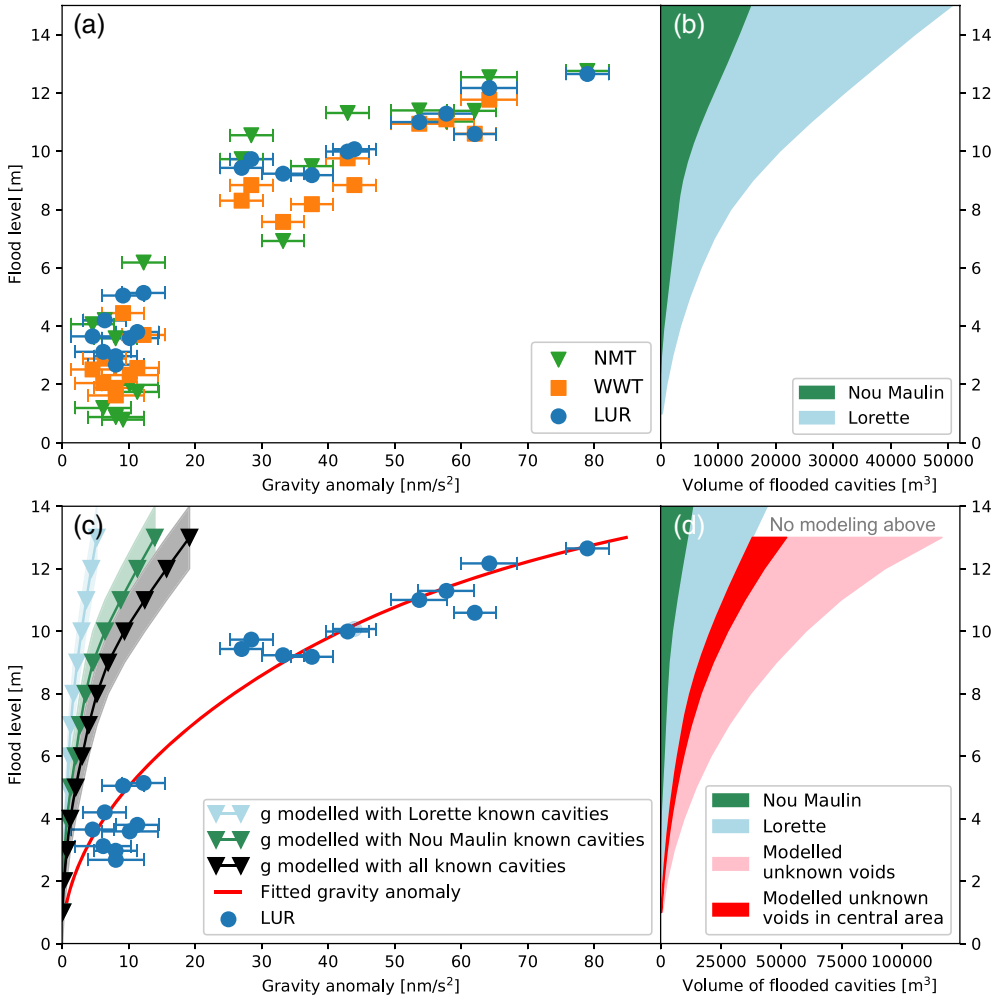

Figure 6. (a) Representation of the highest water level and Δg_{end_max} measured during each flood event, for the LUR (circles), NMT (triangles), and WWT (squares) underground water-level sensors. The error bars illustrate the noise of the gravity measurements. (b) The volume of flooded cavities when accounting for the mapped Nou Maulin and Lorette caves (green and blue, respectively). (c) Similar representation as (a) with data from the LUR water-level sensor (circles) only, to which modeled gravity responses of infiltrating rainwater and rising base level of the epiphreatic zone have been removed. (d) Similar representation as (b) plus the modeled additional voids distributed either in the whole modeled area (pink) or within the central part of the Lorette cave (red).

Calculations for a second scenario in which the unknown voids are to find in the central part of the Lorette Cave results in only 14,160 m^3 of additional unknown cavities. This seems more realistic as it amounts half of the volume being flooded in the known cavities of the northern unit. As a comparison, this is 1.5 times bigger than the Val d'Enfer chamber, at the center of Lorette cave, which has a size estimated to 10,000 m^3 (Triantafyllou et al., 2019). Several points support this hypothesis.

The first point was initially raised to explain the dynamic of the flood in section 4.2. It concerns the outcropping width of both units, also represented by the area covered by both units in the sampling volume of the gravimeter, as shown in Figure 1 (76.7% and 23.3% for the southern and the northern units, respectively). The total volume of cavities being flooded in the Lorette Cave is also 2.2 times greater than for the Nou Maulin Cave. However, the contributions of the cavities from the Lorette Cave to the modeled gravity signal (Figure 6c) is, for the 13-m floods, 2.7 times lower than for the Nou Maulin Cave. This is because the topography of the caves is such that the areas flooded in the Lorette Cave are farther from the gravimeter than those of the Nou Maulin Cave, as shown in Figure 7. In order to estimate which units could host most of the unknown voids, we modeled the evolution of the gravity anomaly during the July 2014 flood. To model Case T1 on Figure 4c, we set a water elevation of 11 m in Nou Maulin Cave and of 7 m in Lorette Cave. This gives results of $10.1^{+2.9}_{-2.7}$ $nm.s^{-2}$ (see Figure 6c), which is 3.3 times lower than the measured gravity increase

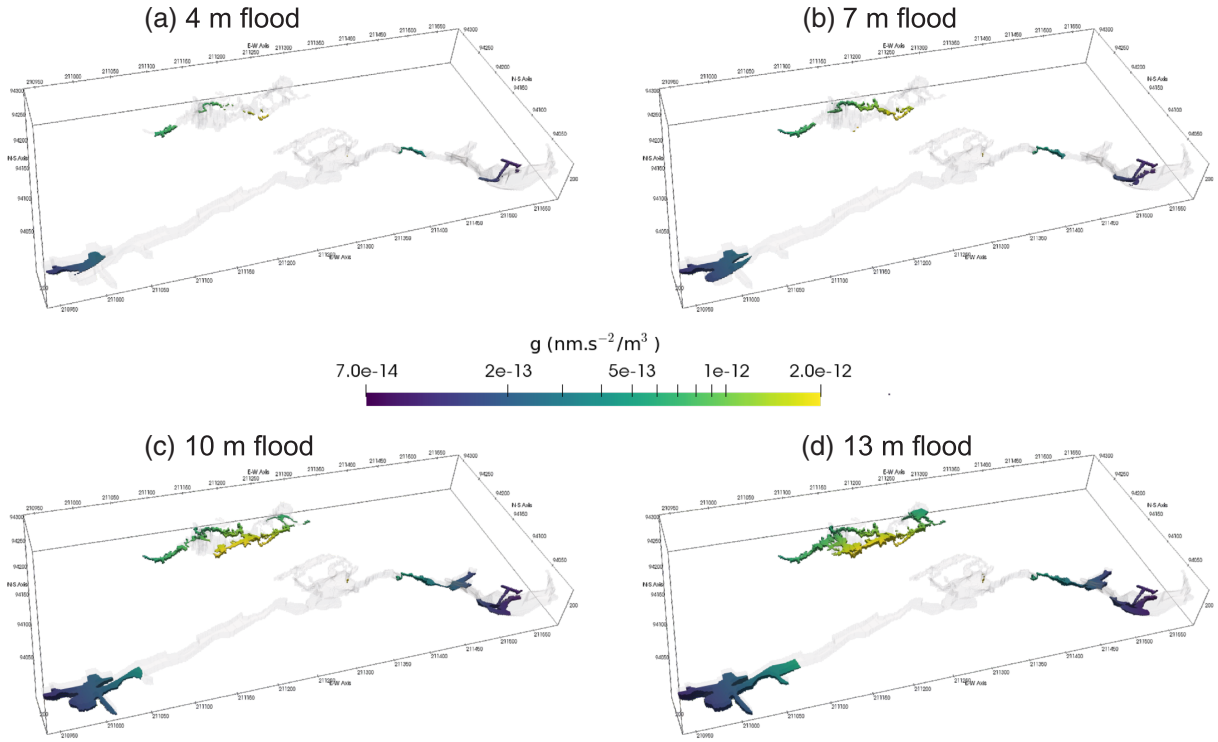

Figure 7. Simulation of 1-, 5-, 9-, and 13-m high floods in the caves. The yellow zone corresponds to the alluvial plain of the Lomme River that is also flooded, producing negligible gravity variations in the simulations.

(42.5 ± 3.2 nm.s^{-2}), to which the modeled rainwater infiltration (9.7 ± 5.2 nm.s^{-2}) is subtracted. While keeping the 11-m level in Nou Maulin Cave, the rising water level from 7 to 11.3 m in Lorette Cave is modeled to an increase of $+2.3^{+1.1}_{-1.0}$ nm.s^{-2}, which is 8.2 times lower than the measured gravity increase minus the modeled rainwater contribution (+18.8 ± 3.2 nm.s^{-2}) in July 2014 (see Table S2 in the supporting information). This is significantly higher and suggests the presence of additional water masses in the southern unit.

The second point supporting the hypothesis that a majority of the unmapped voids are concentrated in the southern unit focuses on the morphology of both caves. Lorette cave contains only very few reported passages below 176-m AOD (Figure 1c) in its middle section, that is, above the level reached by the 13-m flood events. This is emphasized in Figure 8 which maps out a flood event along a cross section of the Lorette cave, showing this lack of mapped cavities in deep areas of the central part and the modeled cavities. Additional conduits are thus necessary to transfer water from the eastern cavities to the western passages, and both areas are known to have floors below 170 m AOD (i.e., the altitude of an 8-m flood). In contrast, the floors of the mapped Nou Maulin passages are all located below 170-m AOD and the connectivity between all the areas flooded is attested for floods over 6 m. Fewer additional voids are therefore required in this case to ensure the underground drainage.

These arguments support the hypothesis that a major network of passages or connected voids is located in the middle part of the Lorette Cave, below the level of the mapped cavities (Figure 8). This is corroborated by the formation process of the central chamber of the Lorette Cave (Val d'Enfer), which is the result of two sinkhole collapses, as discernible from the Lidar topography in Figure 1c. Two flanks of the chamber host massive scree slopes terminating on flat ground. Our interpretation is that these scree slopes are larger and deeper and extend beyond the surface of the ground, which is likely to comprise of fill material as a result of the collapses. The scree would therefore host plenty of small connected voids acting as drains helping the allogeneic water to flow to the western part of the cave and would potentially hide an undiscovered block-field cave chamber. The existence of U-bend conduits could counter this hypothesis, but no evidence

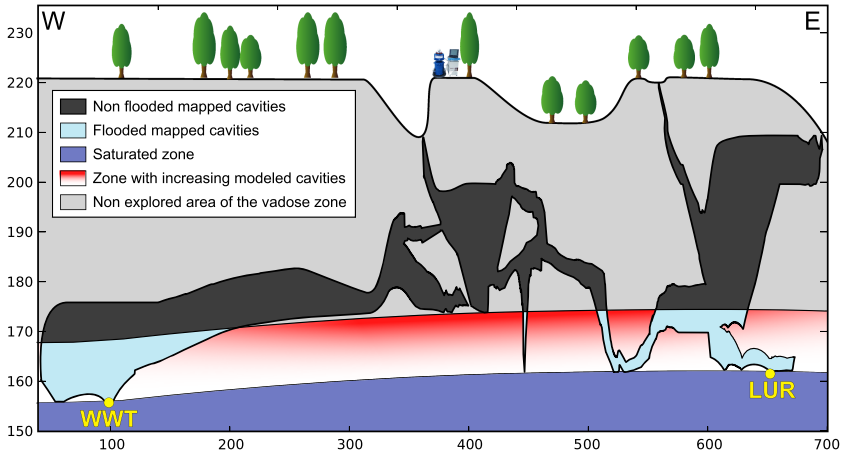

Figure 8. Conceptual model of a 13-m flood event in the Lorette cave projected on a west–east cross section. The zone progressively shifting from white to red represents the layer in which the modeled cavities are located. Red indicates a greater number of cavities. LUR and WWT refer to the water level sensor of Figure 1c.

of such systems has been found nor could be explained by the local geology. The only siphon-like system reported in the area is located at the resurgence of the Lomme Karst System, 7-km east of the field site.

It is likely that increasing water level would favor poorly connected voids to be affected by the flood, although this hypothesis would be practically impossible to differentiate from the aforementioned scenario. An intense campaign of relative gravity measurements, made with a Scintrex CG5 gravimeter, in surface and at depth, similar to that developed by Jacob et al. (2009), could have been useful to inform on the porosity of the massif at different depths. Although a similar approach was implemented at the RCL site, acquiring 35 surveys over 2 years, it was difficult to distinguish a hydrological signal from the noise level of the CG5 gravimeter (typically around 50 $nm.s^{-2}$) given the relatively small surface area and, thus, small expected lateral variations.

6. Conclusions

This research aimed at investigating karst hydrological characteristics of underground flash floods at the RCL site in the Rochefort karst system, in a temperate maritime climate. Twenty flood events could be utilized to study the dynamic of the flood and their resulting gravity anomalies of several tens of $nm.s^{-2}$. The analyses of such flash flood events monitored with four water-level sensors and one single surface gravimeter lead to detect unknown voids in the subsurface and eventually present a likely location for them in the system.

First, we analyzed the gravity signals associated with the floods and identified persistent gravity increases after each flood. We demonstrated that the source of such a gravity step can be explained by the infiltration of local rainwater in the massif and is not a consequence of any flood-induced recharge of the aquifer. This is different to the results found by Jourde et al. (2014), which identified a direct recharge of the karst saturated zone following flood events in a Mediterranean context and in certain conditions. Our study focuses on a humid karst which may explain the difference in findings from Jourde et al. (2014). This difference highlights how much climate characteristics and karst morphology affect aquifer recharge, as has been assumed in several studies (Hartmann et al., 2014; Klimchouk, 2004). Moreover, our results demonstrate the effect of intense rainfall and extreme weather events on the recharge of the karst vadose zone itself. This may have an impact on the recharge of the saturated zone of the aquifer, as either a delayed response (Bakalowicz, 2005; Clemens et al., 1999) or provide inputs to permanent storage within the vadose zone (Arbel et al., 2010; Williams, 2008).

In addition to this, we revealed the morphological characteristics of the underground, that is, the number of connected voids in an environment as complex as a karst system. The cavities of our test site are already extensively mapped but a major proportion of unmapped voids have been inferred. To reproduce the

observed gravity anomaly, between 14,160 and 78,520 m^3 of additional voids are required, distributed either in the central part of the Lorette Cave, as supported by geological and morphological information, or in all of the high sensitivity area of the gravimeter. This is in addition to the mapped passages being flooded, which is estimated as 38,000 m^3. As such, the workflow used for this study may be of interest to those assessing subsurface properties in other cave systems worldwide that exhibit similar flooding events. It could also be adapted to a series of comparable case studies. This involves tide effects in coastal karst areas, hydrothermal processes, magma and fluid migration in volcanic environments, effective rainfalls infiltration, or fluid leakage in porous media.

The added value of gravity measurements to conventional hydrological monitoring is clearly demonstrated in our study. It calls for a greater integration of geophysical measurements within in situ monitoring approaches aiming at improving our knowledge of karst hydrological processes. Gravity monitoring can provide crucial data for studying at the mesoscale seasonal discharge and recharge processes in the karst systems, thereby providing a supporting tool for point sensor networks, which may be limited by heterogeneities within complex systems.

Acknowledgments
This work is part of the Karst Aquifer Research by Geophysics project (http://www.karag.be) funded by the Fonds de la Recherche Scientifique. A. Watlet is also supported by the Ernest du Bois Fund, managed by the King Baudouin Foundation. We would like to thank all the colleagues who were involved in this project and most particularly C. Barcella, S. Castelein, B. Frederick, T. Lecocq, A. Triantafyllou, and K. Van Noten as well as G. Evrard, C. Vanderlinden, and the team members of the ASBL Grottes de Lorette, and the municipality of Rochefort for their hospitality. We thank also all the cavers involved in the Rochefort caves mappings and especially the topography of J.-L. De Bock (1978), S.C. Rochefortois (J. Dehove, J.-L. Nandance and J.-M. Renier), S.C. Les Fistuleuses (W. Adriaenssen and M. Legros), P. Vandersleyen (1959), the Cerlce des Sciences of Athénée Royal de Rochefort and Birkhoff, E., R. Bollaert, J. Burgers, L. de Graauw, M. Dikstra, M. Legros, G. De Sadelaer, and S. Schaballie (2013). We are thankful to two anonymous reviewers for their rigorous comments which greatly helped to improve this study, as well as J. Whiteley for the greatly appreciated proof reading. This paper benefits from Matplotlib (Hunter, 20072007), Pandas (McKinney, 20112011), and GDAL/OGR packages (available at http://gdal.osgeo.org) as well as QGis (available at http://qgis.osgeo.org) and Tsoft (Van Camp & Vauterin, 20052005) software. Data of the SLR water level sensor are available at http://aqualim.environnement.wallonie.be/Station.do?method=selectStation&station=L6650 website. Other data used for this study are available in the supporting information. A. Watlet publishes with the permission of the Executive Director, British Geological Survey (UKRI-NERC).

References

Arbel, Y., Greenbaum, N., Lange, J., & Inbar, M. (2010). Infiltration processes and flow rates in developed karst vadose zone using tracers in cave drips. *Earth Surface Processes and Landforms*, *35*(14), 1682–1693. https://doi.org/10.1002/esp.2010

Atkinson, T. C. (1977). Diffuse flow and conduit flow in limestone terrain in the Mendip Hills, Somerset (Great Britain). *Journal of Hydrology*, *35*(1–2), 93–110. https://doi.org/10.1016/0022-1694(77)90079-8

Bakalowicz, M. (2005). Karst groundwater: A challenge for new resources. *Hydrogeology Journal*, *13*(1), 148–160. https://doi.org/10.1007/s10040-004-0402-9

Barchy, L., Dejonghe, L., & Marion, J.-M. (2014). Rochefort-Nassogne N°59/3–4, Carte géologique de Wallonie.

Birkhoff, E., Bollaert, R., Burgers, J., de Graauw, L., Dikstra, M., & Legros, M. (2013). Nouvelle topographie de la Grotte du Nou Maulin, http://noumaulin.blogspot.com. www.noumaulin.blogspot.com.

Blöschl, G., & Sivapalan, M. (1995). Scale issues in hydrological modelling: A review. *Hydrological Processes*, *9*(3–4), 251–290. Retrieved from. http://onlinelibrary.wiley.com/doi/10.1002/hyp.3360090305/full

Boggs, P. T., Boggs, P. T., Rogers, J. E., & Schnabel, R. B. (1992). User's reference guide for odrpack version 2.01: Software for weighted orthogonal distance regression.

Bonacci, O., Ljubenkov, I., & Roje-Bonacci, T. (2006). Karst flash floods: An example from the Dinaric karst (Croatia). *Natural Hazards and Earth System Sciences*, *6*(2), 195–203. Retrieved from. https://hal.archives-ouvertes.fr/hal-00299276/

Boy, J.-P., & Hinderer, J. (2006). Study of the seasonal gravity signal in superconducting gravimeter data. *Journal of Geodynamics*, *41*(1–3), 227–233. https://doi.org/10.1016/j.jog.2005.08.035

Camelbeeck, T., van Ruymbeke, M., Quinif, Y., Vandycke, S., de Kerchove, E., & Ping, Z. (2011). Observation and interpretation of fault activity in the Rochefort cave (Belgium). *Tectonophysics*, *581*, 48–61. https://doi.org/10.1016/j.tecto.2011.09.027

Caratori Tontini, F., de Ronde, C. E. J., Scott, B. J., Soengkono, S., Stagpoole, V., Timm, C., & Tivey, M. (2016). Interpretation of gravity and magnetic anomalies at Lake Rotomahana: Geological and hydrothermal implications. *Journal of Volcanology and Geothermal Research*, *314*, 84–94. https://doi.org/10.1016/j.jvolgeores.2015.07.002

Chalikakis, K., Plagnes, V., Guerin, R., Valois, R., & Bosch, F. P. (2011). Contribution of geophysical methods to karst-system exploration: An overview. *Hydrogeology Journal*, *19*(6), 1169–1180. https://doi.org/10.1007/s10040-011-0746-x

Clemens, T., Hückinghaus, D., Liedl, R., & Sauter, M. (1999). Simulation of the development of karst aquifers: Role of the epikarst. *International Journal of Earth Sciences*, *88*(1), 157–162. Retrieved from. http://www.springerlink.com/index/H3NA9V27KDCVNT8C.pdf

Creutzfeldt, B., Güntner, A., Klügel, T., & Wziontek, H. (2008). Simulating the influence of water storage changes on the superconducting gravimeter of the geodetic observatory Wettzell, Germany. *Geophysics*, *73*(6), WA95–WA104. https://doi.org/10.1190/1.2992508

Creutzfeldt, B., Güntner, A., Wziontek, H., & Merz, B. (2010). Reducing local hydrology from high-precision gravity measurements: A lysimeter-based approach: Reducing hydrology from gravity measurements. *Geophysical Journal International*, *183*(1), 178–187. https://doi.org/10.1111/j.1365-246X.2010.04742.x

Creutzfeldt, B., Troch, P. A., Güntner, A., Ferré, T. P. A., Graeff, T., & Merz, B. (2014). Storage-discharge relationships at different catchment scales based on local high-precision gravimetry. *Hydrological Processes*, *28*(3), 1465–1475. https://doi.org/10.1002/hyp.9689

Deville, S. (2013). Caractérisation de la zone non saturée des karsts par la gravimétrie et l'hydrogéologie (Ph.D. thesis). Université Montpellier II-Sciences et Techniques du Languedoc, Montpellier, France.

Deville, S., Jacob, T., Chery, J., & Champollion, C. (2012). On the impact of topography and building mask on time varying gravity due to local hydrology. *Geophysical Journal International*, *192*(1), 82–93. https://doi.org/10.1093/gji/ggs007

Dikstra, M., & Burgers, J. (2015). La Grotte du Nou Maulin. *Regards*, *80*, 4–15.

Dubois, Y. (1993). Le Nou Maulin. *Regards*, *11*, 1–10.

Fores, B. (2016). Gravimétrie et surveillance sismique pour la modélisation hydrologique en milieu karstique. Application au bassin du Durzon (Larzac, France) (Ph.D. thesis). Université de Montpellier, Montpellier, France.

Fores, B., Champollion, C., Le Moigne, N., Bayer, R., & Chéry, J. (2016). Assessing the precision of the iGrav superconducting gravimeter for hydrological models and karstic hydrological process identification. *Geophysical Journal International*, *208*(1), 269–280. https://doi.org/10.1093/gji/ggw396

Fores, B., Klein, G., Le Moigne, N., & Francis, O. (2019). Long-term stability of tilt-controlled gPhoneX gravimeters. *Journal of Geophysical Research - Solid Earth*, *124*, 12,264–12,276. https://doi.org/10.1029/2019JB018276

Francis, O., Van Camp, M., van Dam, T., Warnant, R., & Hendrickx, M. (2004). Indication of the uplift of the Ardenne in long-term gravity variations in Membach (Belgium). *Geophysical Journal International*, *158*(1), 346–352. https://doi.org/10.1111/j.1365-246X.2004.02310.x

Goldscheider, N., & Drew, D. P. (2007). *Methods in karst hydrogeology*. London: Taylor & Francis.
Güntner, A., Reich, M., Mikolaj, M., Creutzfeldt, B., Schroeder, S., & Wziontek, H. (2017). Landscape-scale water balance monitoring with an iGrav superconducting gravimeter in a field enclosure. *Hydrology and Earth System Sciences Discussions*, 1–28. https://doi.org/10.5194/hess-2017-103
Hartmann, A., Gleeson, T., Rosolem, R., Pianosi, F., Wada, Y., & Wagener, T. (2015). A large-scale simulation model to assess karstic groundwater recharge over Europe and the Mediterranean. *Geoscientific Model Development*, *8*(6), 1729–1746. https://doi.org/10.5194/gmd-8-1729-2015
Hartmann, A., Goldscheider, N., Wagener, T., Lange, J., & Weiler, M. (2014). Karst water resources in a changing world: Review of hydrological modeling approaches. *Reviews of Geophysics*, *52*, 218–242. https://doi.org/10.1002/2013RG000443
Hasan, S., Troch, P. A., Bogaart, P. W., & Kroner, C. (2008). Evaluating catchment-scale hydrological modeling by means of terrestrial gravity observations: Gravity and hydrology. *Water Resources Research*, *44*, W08416. https://doi.org/10.1029/2007WR006321
Heck, B., & Seitz, K. (2007). A comparison of the tesseroid, prism and point-mass approaches for mass reductions in gravity field modelling. *Journal of Geodesy*, *81*(2), 121–136. https://doi.org/10.1007/s00190-006-0094-0
Hemmings, B., Gottsmann, J., Whitaker, F., & Coco, A. (2016). Investigating hydrological contributions to volcano monitoring signals. A time-lapse gravity example. *Geophysical Journal International*, *207*(1), 259–273. https://doi.org/10.1093/gji/ggw266
Hinderer, J., Crossley, D., & Warburton, R. J. (2007). Gravimetric methods-superconducting gravity meters-3.04. In G. Schubert (Ed.), *Treatise on Geophysics*, (pp. 65–122). Amsterdam: Elsevier.
Hirabayashi, Y., Mahendran, R., Koirala, S., Konoshima, L., Yamazaki, D., Watanabe, S., et al. (2013). Global flood risk under climate change. *Nature Climate Change*, *3*(9), 816–821. https://doi.org/10.1038/nclimate1911
Hunter, J. D. (2007). Matplotlib: A 2D graphics environment. *Computing in Science & Engineering*, *9*(3), 90–95. https://doi.org/10.1109/MCSE.2007.55
Imanishi, Y., Kokubo, K., & Tatehata, H. (2006). Effect of underground water on gravity observation at Matsushiro, Japan. *Journal of Geodynamics*, *41*(1–3), 221–226. https://doi.org/10.1016/j.jog.2005.08.031
Jacob, T., Bayer, R., Chery, J., Jourde, H., Moigne, N. L., Boy, J.-P., et al. (2008). Absolute gravity monitoring of water storage variation in a karst aquifer on the larzac plateau (Southern France). *Journal of Hydrology*, *359*(1–2), 105–117. https://doi.org/10.1016/j.jhydrol.2008.06.020
Jacob, T., Chery, J., Bayer, R., Le Moigne, N., Boy, J.-P., Vernant, P., & Boudin, F. (2009). Time-lapse surface to depth gravity measurements on a karst system reveal the dominant role of the epikarst as a water storage entity. *Geophysical Journal International*, *177*(2), 347–360. https://doi.org/10.1111/j.1365-246X.2009.04118.x
Jourde, H., Lafare, A., Mazzilli, N., Belaud, G., Neppel, L., Dörfliger, N., & Cernesson, F. (2014). Flash flood mitigation as a positive consequence of anthropogenic forcing on the groundwater resource in a karst catchment. *Environmental Earth Sciences*, *71*(2), 573–583.
Kennedy, J., Ferré, T. P. A., & Creutzfeldt, B. (2016). Time-lapse gravity data for monitoring and modeling artificial recharge through a thick unsaturated zone. *Water Resources Research*, *52*, 7244–7261. https://doi.org/10.1002/2016WR018770
Klimchouk, A. (2004). Towards defining, delimiting and classifying epikarst: Its origin, processes and variants of geomorphic evolution. *Speleogenesis and Evolution of Karst Aquifers*, *2*(1), 1–13. Retrieved from. http://speleogenesis.info/pdf/SG5/SG5_artId3263.pdf
Lampitelli, C., & Francis, O. (2010). Hydrological effects on gravity and correlations between gravitational variations and level of the Alzette River at the station of Walferdange, Luxembourg. *Journal of Geodynamics*, *49*(1), 31–38. Retrieved from. http://www.sciencedirect.com/science/article/pii/S0264370709000660
Legros, M., Nandance, J.-L., Pauwels, M., Quinif, Y., & Maboge, B. (1993). La nouvelle galerie de Rochefort. *Regards*, *11*, 18–22.
Leirião, S., He, X., Christiansen, L., Andersen, O. B., & Bauer-Gottwein, P. (2009). Calculation of the temporal gravity variation from spatially variable water storage change in soils and aquifers. *Journal of Hydrology*, *365*(3–4), 302–309. https://doi.org/10.1016/j.jhydrol.2008.11.040
Li, X., & Chouteau, M. (1998). Three-dimensional gravity modeling in all space. *Surveys in Geophysics*, *19*(4), 339–368. https://doi.org/10.1023/A:1006554408567
Longuevergne, L., Boy, J. P., Florsch, N., Viville, D., Ferhat, G., Ulrich, P., et al. (2009). Local and global hydrological contributions to gravity variations observed in Strasbourg. *Journal of Geodynamics*, *48*(3-5), 189–194. Retrieved from. http://www.sciencedirect.com/science/article/pii/S0264370709000751, https://doi.org/10.1016/j.jog.2009.09.008
MacMillan, W. D. (1958). *The Theory of the Potential*. New York: McGraw-Hill.
Mangin, A. (1975). Contribution à l'étude hydrodynamique des aquifères karstiques (Doctoral dissertation). Dijon, France: Université de Dijon.
McKinney, W. (2011). Pandas: A foundational Python library for data analysis and statistics. Paper presented at the PyHPC 2011, Workshop on Python for High Performance and Scientifc Computing. Seattle, WA.
Merriam, J. B. (1992). Atmospheric pressure and gravity. *Geophysical Journal International*, *109*(3), 488–500. https://doi.org/10.1111/j.1365-246X.1992.tb00112.x
Meurers, B., Van Camp, M., & Petermans, T. (2007). Correcting superconducting gravity time-series using rainfall modelling at the Vienna and Membach stations and application to Earth tide analysis. *Journal of Geodesy*, *81*(11), 703–712. https://doi.org/10.1007/s00190-007-0137-1
Mikolaj, M., Meurers, B., & Güntner, A. (2016). Modelling of global mass effects in hydrology, atmosphere and oceans on surface gravity. *Computers & Geosciences*, *93*, 12–20. https://doi.org/10.1016/j.cageo.2016.04.014
Mikolaj, M., Meurers, B., & Mojzeš, M. (2015). The reduction of hydrology-induced gravity variations at sites with insufficient hydrological instrumentation. *Studia Geophysica et Geodaetica*, *59*(3), 424–437. https://doi.org/10.1007/s11200-014-0232-8
Mikolaj, M., Reich, M., & Güntner, A. (2019). resolving geophysical signals by terrestrial gravimetry: A time domain assessment of the correction-induced uncertainty. *Journal of Geophysical Research - Solid Earth*, *124*, 2153–2165. https://doi.org/10.1029/2018JB016682
Nagy, D. (1966). The gravitational attraction of a right rectangular prism. *Geophysics*, *31*(2), 362–371. https://doi.org/10.1190/1.1439779
Naujoks, M., Kroner, C., Weise, A., Jahr, T., Krause, P., & Eisner, S. (2010). Evaluating local hydrological modelling by temporal gravity observations and a gravimetric three-dimensional model: Gravity and hydrology: Local 3-D modelling. *Geophysical Journal International*. https://doi.org/10.1111/j.1365-246X.2010.04615.x
Okabe, M. (1979). Analytical expressions for gravity anomalies due to homogeneous polyhedral bodies and translations into magnetic anomalies. *Geophysics*, *44*(4), 730–741. https://doi.org/10.1190/1.1440973
Poulain, A. (2017). Flow and transport characterization in vadose and phreatic zones of karst aquifers: Experimental approaches in the Givetian limestones of South Belgium (Doctoral dissertation). Namur, Belgium: Université de Namur.

Poulain, A., Watlet, A., Kaufmann, O., Van Camp, M., Jourde, H., Mazzilli, N., et al. (2018). Assessment of groundwater recharge processes through karst vadose zone by cave percolation monitoring. *Hydrological Processes*, *32*(13), 2069–2083. https://doi.org/10.1002/hyp.13138

Quinif, Y. (2016). Etagement dans la grotte de Lorette-Relation avec les dépôts souterrains. *Regards*, *81*, 60–69. Retrieved from http://www.google.com/url?sa=t&rct=j&q=&esrc=s&source=web&cd=1&ved=0ahUKEwjak6zyocbOAhUHJMAKHeCnDKcQFggcMAA&url=http%3A%2F%2Fwww.cdiscount.com%2Fle-sport%2Fr-colle%2Brustine.html&usg=AFQjCNEyQFQU8QNBdGM_Z-gjcPHon7fGcA&sig2=7KWwAGii4Bm0M4TBEQkG6Q&bvm=bv.129759880,d.ZGg

Quinif, Y., Van Ruymbeke, M., Camelbeek, T., & Vandycke, S. (1997). Les failles actives de la Grotte de Rocheforrt (Ardenne, Belgique) sont-elles sismogéniques? Installation d'un laboratoire souterrain. *Aardkundige Mededelingen*, *8*, 153–156.

Reich, M., Mikolaj, M., Blume, T., & Güntner, A. (2019). Reducing gravity data for the influence of water storage variations beneath observatory buildings. *Geophysics*, *84*(1), EN15–EN31.

Riccardi, U., Rosat, S., & Hinderer, J. (2011). Comparison of the micro-g LaCoste gPhone-054 spring gravimeter and the GWR-C026 superconducting gravimeter in Strasbourg (France) using a 300-day time series. *Metrologia*, *48*(1), 28–39. https://doi.org/10.1088/0026-1394/48/1/003

Sekowski, M., Dykowski, P., & Krynski, J. (2016). A new superconducting gravimeter station in Central Europe: The iGrav-027 at the Borowa Gora Geodetic-Geophysical Observatory–installation and first results. *Geoinformation Issues*, *8*(1), 5–17. Retrieved from https://www.researchgate.net/profile/Jan_Krynski/publication/314950674_A_new_superconducting_gravimeter_station_in_Central_Europe_the_iGrav-027_at_the_Borowa_Gora_Geodetic-Geophysical_Observatory_-_installation_and_first_results/links/58c7b90c458515478dcdc19d/A-new-superconducting-gravimeter-station-in-Central-Europe-the-iGrav-027-at-the-Borowa-Gora-Geodetic-Geophysical-Observatory-installation-and-first-results.pdf

Smart, P. L., & Friederich, H. (1987). Water movement and storage in the unsaturated zone of a maturely karstified carbonate aquifer, Mendip Hills, England. In *Proceedings of the Environmental Problems in Karst Terranes and their Solutions*, (pp. 59–87). Dublin, Ohio: National Water Well Association.

Takemoto, S., Fukuda, Y., Higashi, T., Ogasawara, S., Abe, M., Dwipa, S., et al. (2002). Effect of groundwater changes on SG observations in Kyoto and Bandung. *Bulletin d'Informations Des Marees Terrestres*, *10*, 839–810.

Triantafyllou, A., Watlet, A., Le Mouélic, S., Camelbeeck, T., Civet, F., Kaufmann, O., et al. (2019). 3-D digital outcrop model for analysis of brittle deformation and lithological mapping (Lorette cave, Belgium). *Journal of Structural Geology*, *120*, 55–66. https://doi.org/10.1016/j.jsg.2019.01.001

Van Camp, M. (2005). Uncertainty of absolute gravity measurements. *Journal of Geophysical Research*, *110*, B05406. https://doi.org/10.1029/2004JB003497

Van Camp, M., de Viron, O., Pajot-Métivier, G., Casenave, F., Watlet, A., Dassargues, A., & Vanclooster, M. (2016). Direct measurement of evapotranspiration from a forest using a superconducting gravimeter: Evapotranspiration and gravity. *Geophysical Research Letters*, *43*, 10,225–10,231. https://doi.org/10.1002/2016GL070534

Van Camp, M., de Viron, O., & Warburton, R. J. (2013). Improving the determination of the gravity rate of change by combining superconducting with absolute gravimeter data. *Computers & Geosciences*, *51*, 49–55. https://doi.org/10.1016/j.cageo.2012.07.029

Van Camp, M., de Viron, O., Watlet, A., Meurers, B., Francis, O., & Caudron, C. (2017). Geophysics from terrestrial time-variable gravity measurements. *Reviews of Geophysics*, *55*, 938–992. https://doi.org/10.1002/2017RG000566

Van Camp, M., Meurers, B., de Viron, O., & Forbriger, T. (2016). Optimized strategy for the calibration of superconducting gravimeters at the one per mille level. *Journal of Geodesy*, *90*(1), 91–99. https://doi.org/10.1007/s00190-015-0856-7

Van Camp, M., Meus, P., Quinif, Y., Kaufmann, O., Ruymbeke, M., Vandiepenbeck, M., & Camelbeeck, T. (2006). Karst aquifer investigation using absolute gravity. *Eos, Transactions American Geophysical Union*, *87*(30), 298–298. https://doi.org/10.1029/2006EO300005

Van Camp, M., & Vauterin, P. (2005). Tsoft: Graphical and interactive software for the analysis of time series and earth tides. *Computers & Geosciences*, *31*(5), 631–640. https://doi.org/10.1016/j.cageo.2004.11.015

Van Camp, M., Viron, O. d., Metivier, L., Meurers, B., & Francis, O. (2014). The quest for a consistent signal in ground and GRACE gravity time-series. *Geophysical Journal International*, *197*(1), 192–201. https://doi.org/10.1093/gji/ggt524

Warburton, R. J., Pillai, H., & Reineman, R. C. (2010). Initial results with the new GWR iGrav superconducting gravity meter. In *International Association of Geodesy (IAG) Symposium Proceedings, Russia, Saint Petersbourg*.

Watlet, A. (2017). Hydrogeophysical monitoring of groundwater recharge processes through the karst vadose zone at Rochefort (Belgium). University of Mons.

Watlet, A., Kaufmann, O., Triantafyllou, A., Poulain, A., Chambers, J. E., Meldrum, P. I., et al. (2018). Imaging groundwater infiltration dynamics in the karst vadose zone with long-term ERT monitoring. *Hydrology and Earth System Sciences*, *22*(2), 1563–1592. https://doi.org/10.5194/hess-22-1563-2018

White, W. B. (2002). Karst hydrology: Recent developments and open questions. *Engineering Geology*, *65*(2), 85–105. Retrieved from. http://www.sciencedirect.com/science/article/pii/S0013795201001168

Williams, P. W. (2008). The role of the epikarst in karst and cave hydrogeology: A review. *International Journal of Speleology*, *37*(1), 1. Retrieved from. http://scholarcommons.usf.edu/ijs/vol37/iss1/1/

Wilson, C. R., Scanlon, B., Sharp, J., Longuevergne, L., & Wu, H. (2012). Field test of the superconducting gravimeter as a hydrologic sensor. *Ground Water*, *50*(3), 442–449. https://doi.org/10.1111/j.1745-6584.2011.00864.x

Woods, R. (2006). Hydrologic concepts of variability and scale. In *Encyclopedia of Hydrological Sciences* (pp. 23–40). M. G. Anderson et al. (Eds.), J. Wiley & Sons, Chichester.